Oxidative Metabolites Accelerate Alzheimer's Amyloidogenesis by a Two-Step Mechanism, Eliminating the Requirement for Nucleation†

Jan Bieschke, Qinghai Zhang, Evan T. Powers, Richard A. Lerner, and Jeffery W. Kelly*

The Scripps Research Institute and The Skaggs Institute for Chemical Biology, 10550 North Torrey Pines Road, La Jolla, California 92037

Received January 18, 2005; Revised Manuscript Received February 17, 2005

ABSTRACT: The process of amyloid formation by the amyloid β peptide (Aβ), i.e., the misassembly of Aβ peptides into soluble quaternary structures and, ultimately, amyloid fibrils, appears to be at the center of Alzheimer's disease (AD) pathology. We have shown that abnormal oxidative metabolites, including cholesterol-derived aldehydes, modify Aβ and accelerate the early stages of amyloidogenesis (the formation of spherical aggregates). This process, which we have termed metabolite-initiated protein misfolding, could explain why hypercholesterolemia and inflammation are risk factors for sporadic AD. Herein, the mechanism by which cholesterol metabolites hasten Aβ 1−40 amyloidogenesis is explored, revealing a process that has at least two steps. In the first step, metabolites modify Aβ peptides by Schiff base formation. The Aβ−metabolite adducts form spherical aggregates by a downhill polymerization that does not require a nucleation step, dramatically accelerating Aβ aggregation. In agitated samples, a second step occurs in which fibrillar aggregates form, a step also accelerated by cholesterol metabolites. However, the metabolites do not affect the rate of fibril growth in seeded aggregation assays; their role appears to be in initiating amyloidogenesis by lowering the critical concentration for aggregation into the nanomolar range. Small molecules that block Schiff base formation inhibit the metabolite effect, demonstrating the importance of the covalent adduct. Metabolite-initiated amyloidogenesis offers an explanation for how Aβ aggregation could occur at physiological nanomolar concentrations.

Alzheimer's disease (AD)[1] is one of the most common age-associated pathologies, which inevitably leads to dementia and death. AD is strongly linked to the formation of amyloid (a fibrillar, β-sheet-rich aggregate) by the amyloid β peptides (Aβ) (*1*). Aβ is a family of peptides from 39 to 43 residues long with a common N-terminus and a ragged C-terminus. They result from β- and γ-secretase cleavage of the amyloid precursor protein (APP) during secretion (*2*, *3*). A central biophysical mystery of AD is how amyloidogenesis occurs at physiological concentrations of Aβ. The average concentration of Aβ in the human brain is under 10 nM, whereas the critical concentration for Aβ amyloidogenesis in vitro is 1−10 μM (*4*, *5*) (the critical concentration is the concentration below which amyloidogenesis cannot occur). Previous explanations for how Aβ aggregates in the human brain assume that Aβ is concentrated by 3−4 orders of magnitude on membranes or in organelles, or that the critical concentration may be lowered accordingly by pHs < 6 or by divalent metal ions (*6*). We have recently proposed an alternative explanation, whereby covalent adduct formation between Aβ and oxidative metabolites enables Aβ to aggregate at nanomolar concentrations (*7*). Reactive oxygen species produced during inflammation and oxidative stress cause the formation of aldehyde-containing metabolites that can covalently modify proteins through Schiff base formation. We have found that modification of Aβ by some of these metabolites can increase the amyloidogenicity of Aβ (*7*). In particular, Aβ rapidly aggregates in the presence of the recently discovered (*8*) oxidative cholesterol metabolites 3β-hydroxy-5-oxo-5,6 *seco*cholestan-6-al (Figure 1A: **1**) and its aldol product (**2**; note that because **1** is rapidly converted to **2** in the presence of Aβ, we write it hereafter as **1**(**2**)). This process results in spherical aggregates much like those that have been proposed to be the most neurotoxic aggregates on the Aβ amyloidogenesis pathway (*9*−*16*). The critical concentration of Aβ−**1**(**2**) adducts was determined to be less than 100 nM, suggesting that metabolite modification could trigger Aβ aggregation in vivo and therefore may play a role in the pathogenesis of sporadic AD. Because of this observation, the mechanism of action of metabolite-mediated Aβ aggregation merits scrutiny. Herein, we probe the mechanism of Aβ 1−40 amyloidogenesis in the presence of **1**(**2**).

EXPERIMENTAL PROCEDURES (MATERIALS AND METHODS)

Preparation of Seed-Free Aβ. Aβ 1−40 was purchased from Synpep (Dublin, CA). To ensure that Aβ 1−40 solutions were seed-free, they were pretreated as described previously (*7*). Briefly, Aβ 1−40 powder was dissolved in

† We thank the Skaggs Institute of Chemical Biology, the Lita Annenberg Hazen Foundation, the Bundy Foundation, and the Max-Planck Society for financial support.

* Corresponding author: phone: +1-858-784-9605; fax: +1-858-784-9610; e-mail: jkelly@scripps.edu.

[1] Abbreviations: AD, Alzheimer's disease; APP, amyloid precursor protein; AFM, atomic force microscopy; Aβ, amyloid β peptide; Aβ1−40, amyloid peptide with amino acid residues 1−40; CD, circular dichroism; CMC, critical micelle concentration; PBS, phosphate-buffered saline; HPLC, high-performance liquid chromatography; TfT, thioflavin T dye.

10.1021/bi0501030 CCC: $30.25 © 2005 American Chemical Society
Published on Web 03/11/2005

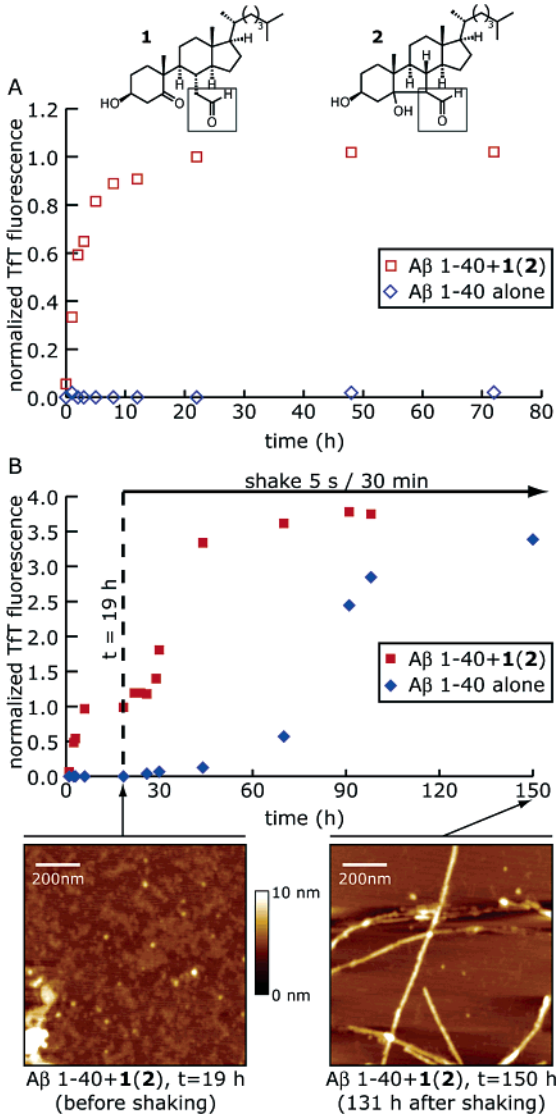

FIGURE 1: (A) Aβ 1−40 (50 μM) aggregation (37 °C, pH 7.4) under quiescent conditions as detected by TfT fluorescence in the presence or absence of **1**(**2**) (50 μM). Fluorescence is normalized to the plateau reached in the presence of **1**(**2**). Inset: structures of 3β-hydroxy-5-oxo-5,6-*seco*cholestan-6-al (**1**) and its aldol product (**2**). (B) Aβ 1−40 aggregation under the conditions described above, except that agitation (5 s of shaking every 30 min) was initiated after 19 h. The AFM images show that small oligomers were present in samples of Aβ 1−40 with **1**(**2**) before agitation (19 h), but fibrils were present at the end point (150 h).

aqueous NaOH (2 mM), and the pH was adjusted to 10.5. This solution was filtered sequentially through 0.2 μm and 10 kD cutoff filters (Millipore, Billerica, MA). Aβ 1−40 solutions prepared in this way showed only one peak by UV absorption in FPLC traces, which, based on the peak area, contained virtually all of the peptide injected onto the column (see Figure 9, Supporting Information). The material in this peak was shown by light scattering (using a Dawn EOS light scattering photometer and the Astra software package; Wyatt Technology, Santa Barbara, CA) to have a molar mass corresponding to monomer (4000 ± 400 g/mol). A similar result was obtained by analytical ultracentrifugation. Aβ 1−40 preparations were stored on ice and used for experiments within 3 h.

Aβ *Amyloidogenesis Assay.* Compound **1**(**2**) in 2-propanol (at 100× the desired final concentration) was diluted 50-fold with phosphate buffer (100 mM sodium phosphate/600 mM NaCl, pH 7.4) containing TfT (40 μM). This solution was added to an equal volume of pretreated Aβ 1−40 at twice the desired final concentration (2−200 μM) in pH 10.5 NaOH. The final solutions contained Aβ 1−40 (1−100 μM), TfT (20 μM), and **1**(**2**) (1−100 μM) in phosphate buffer (50 mM sodium phosphate/300 mM NaCl, pH 7.4) with 1% 2-propanol. Three aliquots (200 μL) of these solutions were transferred into wells of a 96-well microplate for each reaction (Costar black, clear bottom). The plate was sealed and loaded into a Gemini SpectraMax EM fluorescence plate reader (Molecular Devices, Sunnyvale, CA), where it was incubated at 37 °C. The fluorescence (excitation at 440 nm, emission at 485 nm) was measured from the bottom of the plate at 10 or 30 min intervals, with or without 5 s of shaking before each reading. Each data point was the average of 30 scans. Fluorescence traces and t_{50} values represent averages of at least three experiments. Errors were consistently 10% or less of fluorescence values. For normalization, the minimum fluorescence signal was subtracted from all fluorescence values, and the average fluorescence of the plateau phase was defined as 1. In cases in which the slope of the plateau phase fluorescence was not zero, fluorescence was extrapolated to $t = 0$ and the y-intercept was defined as 1.

Aldehyde-sequestering drugs (aminoguanidine, carnosine, pyridoxamine, hydralazine, and methoxyamine) were added from 100× stocks in water to the aggregation buffer to a final concentration of 100 μM for **1**(**2**)-inhibition assays before adding Aβ 1−40 or **1**(**2**). Otherwise, experiments were performed as described above with agitation (5 s of shaking every 10 min).

Atomic Force Microscopy. Aliquots (20 μL) were taken from the assay solutions and adsorbed onto freshly cleaved mica (5 × 5 mm) for 45 s. The liquid was removed by absorption into filter paper. The sample was washed thrice by placing water droplets (20 μL) on the mica surface, and then absorbing them into filter paper. Tapping mode images were obtained on a Digital Instruments multimode scanning probe microscope with a Nanoscope IIIa controller (Veeco, Woodbury, NY).

Circular Dichroism (CD). At selected times, CD spectra of samples prepared as described above were recorded using an AVIV model 202SF CD spectrometer equipped with a Peltier temperature-controlled cell holder using a 0.2 cm path length Suprasil quartz cell (Hellma, Forest Hills, NY). CD spectra were recorded from 200 to 250 nm at 25 °C. The wavelength step size was 0.5 nm, and the averaging time was 1 s at each wavelength.

RESULTS

*Aβ 1−40 Aggregation in the Presence of **1**(**2**) Takes Place in Two Stages in Agitated Assays.* Solutions of Aβ 1−40 (50 μM, pretreated as described in Materials and Methods) with thioflavin T (TfT; a dye that fluoresces upon binding to amyloid fibrils or their precursors; 20 μM) were prepared with and without **1**(**2**) (50 μM). These samples were incubated quiescently at 37 °C and pH 7.4, and the TfT fluorescence [which is proportional to the amount of amyloid or amyloid-like aggregates formed (*17*)] was measured at regular intervals (Figure 1A). TfT-positive aggregates formed rapidly in the presence, but not the absence, of **1**(**2**) (time to

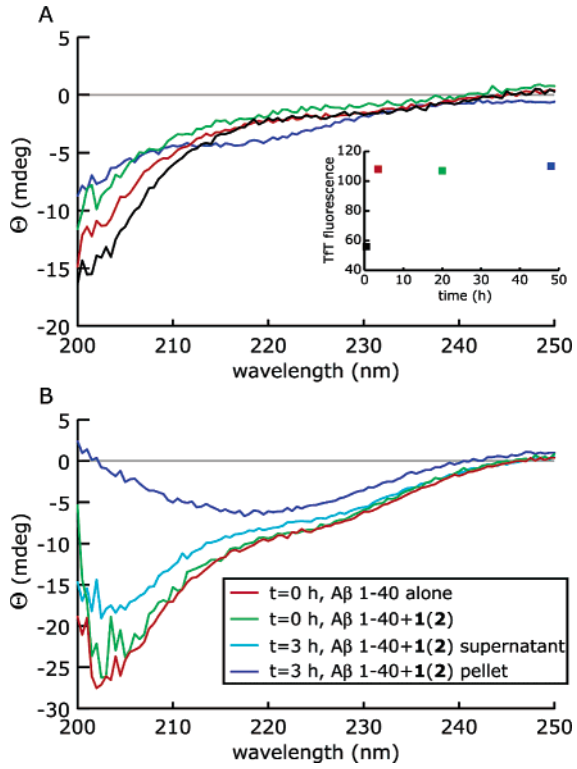

FIGURE 2: (A) CD spectra measured after 30 min (black), 3.5 h (red), 20 h (green), and 48 h (blue) of samples of Aβ 1−40 (20 μM) incubated with an excess of **1**(**2**) (100 μM) at pH 7.4 and 37 °C. Inset: TfT fluorescence (arbitrary units) measured at the time points at which CD spectra were measured. (B) CD spectra obtained at $t = 0$ h of Aβ 1−40 alone (50 μM) or with **1**(**2**) (50 μM). The latter sample was incubated (3 h) and centrifuged (100000*g*), and CD spectra were measured of the material in the supernatant and pellet.

half-maximal fluorescence, or t_{50}, = 3 h). If samples prepared as described above were agitated (5 s of shaking every 30 min) after 19 h of quiescent incubation, then a second stage of aggregation was observed, signaled by a ~4-fold increase in TfT fluorescence (Figure 1B; t_{50} = 16 h after initiating agitation). Small spherical assemblies were produced in the first stage of aggregation, while fibrils were produced in the second stage [Figure 1B, atomic force microscopy (AFM) images]. The second stage of aggregation (but not the first) was observed in the absence of **1**(**2**), but it occurred more slowly (Figure 1B; t_{50} = 64 h after initiating agitation). Roughly 30% of Aβ 1−40 formed aggregates in the presence of **1**(**2**) under quiescent conditions according to analytical gel filtration (See Figure 9B−D, Supporting Information), about half of which was pelleted at 100000*g*. After shaking and reaching the maximum TfT fluorescence, over 90% of the sample was pelleted at 100000*g* (data not shown).

To further characterize the products of the first stage of aggregation, Aβ 1−40 (20 μM) was quiescently incubated with a large excess of **1**(**2**) (100 μM) as described above, and CD spectra and TfT fluorescence were measured at t = 0.5, 3.5, 20, and 48 h (Figure 2A). The first CD spectrum obtained after the TfT fluorescence reached its plateau (t = 3.5 h) showed little difference from that obtained at t = 0.5 h (which was consistent with a random coil). At longer times, however, the ellipticity between 215 and 220 nm became more negative, consistent with an increase in β-sheet content. This suggests that spherical aggregates formed during the first stage of metabolite-initiated Aβ aggregation are rich in β-sheet structure, as expected for species that bind to TfT. To further illustrate this point, Aβ 1−40 (50 μM) was quiescently incubated for 3 h in the presence of **1**(**2**) (50 μM), the sample was centrifuged (100000*g*) for 1 h, the pellet and supernatant were separated, the pellet was resuspended in buffer, and CD spectra of the pellet and the supernatant were measured (Figure 2B). The CD spectrum of the pellet was consistent with peptides in the β-sheet conformation, while the CD spectrum of the supernatant was consistent with an unstructured ensemble.

To determine whether sub-equimolar concentrations of **1**(**2**) can induce two-stage aggregation of Aβ 1−40, solutions of Aβ 1−40 (20 μM) with TfT (20 μM) were prepared at several concentrations of **1**(**2**) (1−100 μM). These samples were incubated at 37 °C and pH 7.4 with agitation (5 s of shaking every 30 min), and the TfT fluorescence was measured (Figure 3A). The amplitude of the first stage depended linearly on the concentration of **1**(**2**) (Figure 3B,C). In contrast, the amplitude of the second stage did not have a clear dependence on the concentration of **1**(**2**), indicating that the second stage reached a similar equilibrium point regardless of the concentration of **1**(**2**) (Figure 3A). The CD spectrum of Aβ 1−40 (20 μM) incubated in the presence **1**(**2**) (20 μM) measured after the second stage was complete (39 h with shaking for 5 s every 30 min; Figure 3D) showed that the structures present at this equilibrium point were predominantly in the β-sheet conformation. Little β-sheet character was observed in the CD spectrum of Aβ 1−40 (50 μM) incubated alone for 39 h (Figure 3D). Concentrations of **1**(**2**) as low as 5 μM were consistently able to induce the second stage of Aβ aggregation (fibrillization) within roughly 24 h. Even at a 1 μM concentration of **1**(**2**), fibrillization of Aβ 1−40 was complete within 24 h in one trial out of three. On this time scale, fibrillization by Aβ 1−40 in the absence of **1**(**2**) is far from complete (Figure 3A).

Atomic force microscopy images of Aβ 1−40 fibrils formed at the end of the second stage of aggregation under the conditions described above without (Figure 4A,B) or with **1**(**2**) (Figure 4C,D) reveals more aggregates in the presence of **1**(**2**) (compare Figure 4, panels A and C). Closer inspection of the fibrils formed with and without **1**(**2**) reveals that they have different morphologies (compare Figure 4, panels B and D). Protofibrils and fibrils are observed in the absence of **1**(**2**), with the latter being best described as a braid of two strands with a repeat length of ~30 nm (Figure 4B). Fibrils formed in the presence of **1**(**2**) have a more complex morphology with a repeat length of 70−80 nm (Figure 4D).

Dependence of the Aggregation Time Scale on Aβ 1−40 Concentration Suggests that the First Stage Is a Downhill Polymerization. Aβ amyloid formation is thought to be a nucleated polymerization, in which the formation of an oligomeric, high-energy nucleus is rate limiting, but once formed the nucleus and fibrils rapidly grow by monomer addition (*18*). A signature characteristic of nucleated polymerizations is a steep increase in the reaction time scale as the initial monomer concentration decreases (time scale $\propto$ [peptide concentration]$^{-n/2}$, where n is the number of monomers in the nucleus). This means that a log−log plot of the time required to reach an arbitrary point in the aggregation reaction (for example, the time required to reach

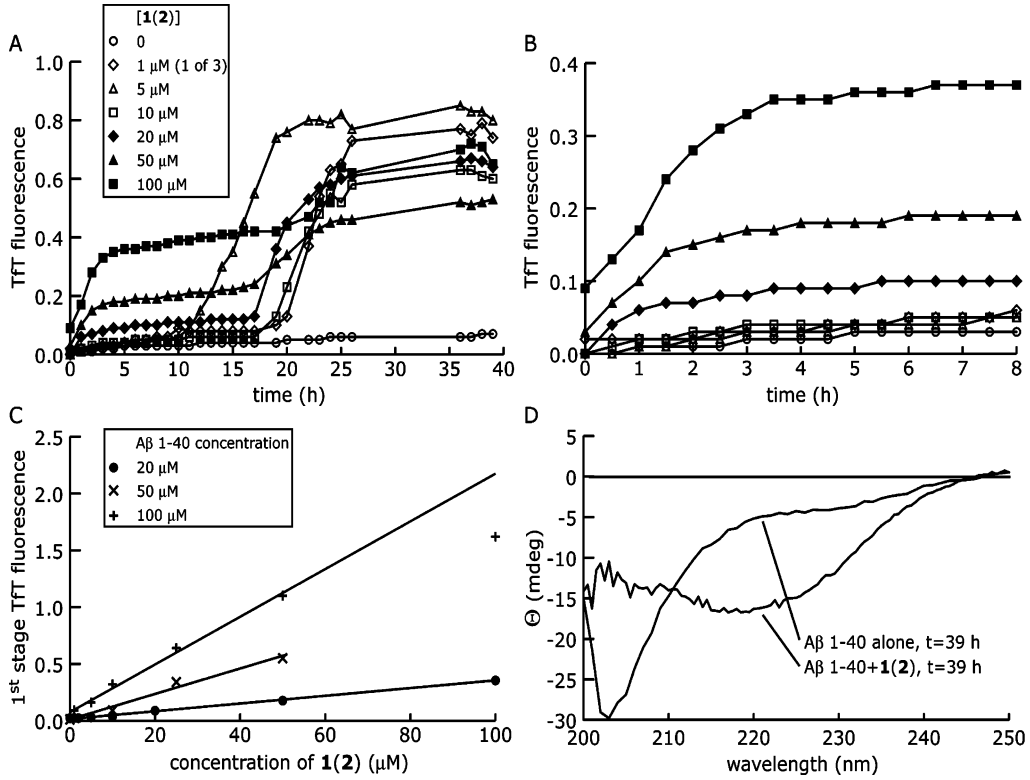

FIGURE 3: (A) Aβ 1−40 (20 μM) aggregation (pH 7.4, 37 °C) with agitation (5 s of shaking every 30 min) in the absence or presence of **1**(**2**) (1−100 μM) as detected by TfT fluorescence (arbitrary units). (B) An expansion of the first 8 h of data from (A). (C) A plot of the TfT fluorescence observed at the end of the first stage of aggregation as a function of the concentration of **1**(**2**) for three concentrations of Aβ 1−40 (20, 50, and 100 μM). The lines are linear fits to the data [the data point at 100 μM of both Aβ 1−40, and **1**(**2**) was an outlier (studentized residual = −7.4)]. (D) CD spectra of Aβ 1−40 (20 μM) incubated for 39 h at pH 7.4, 37 °C with agitation (5 s of shaking every 30 min) in the absence or presence of **1**(**2**) (20 μM).

50% completion, or t_{50}) against the initial Aβ concentration should yield a straight line with a slope of $-n/2$. To determine whether the mechanism of Aβ 1−40 amyloid formation

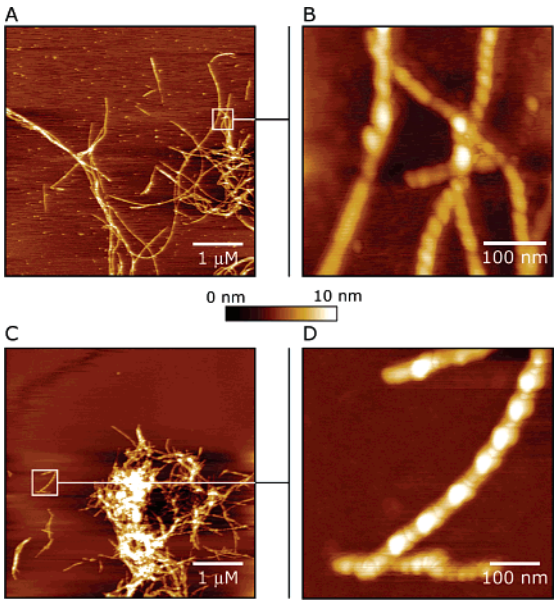

FIGURE 4: (A) AFM image of Aβ 1−40 (20 μM) incubated for 39 h at pH 7.4, 37 °C with agitation (5 s of shaking every 30 min). (B) Expansion of the boxed area in (A). (C) AFM image of Aβ 1−40 (20 μM) incubated for 39 h at pH 7.4, 37 °C with agitation (5 s of shaking every 30 min) in the presence of **1**(**2**) (20 μM). (D) Expansion of the boxed area in panel C.

is a nucleated polymerization, solutions of Aβ 1−40 (5 to 100 μM), thioflavin T (20 μM), and **1**(**2**) (50 μM) were prepared. These samples were incubated at 37 °C and pH 7.4 with agitation (5 s of shaking every 30 min), and the TfT fluorescence was measured (Figure 5A; note that second stage kinetics at $t > 24$ h have been omitted). The logarithm of t_{50} was plotted against the logarithm of Aβ 1−40 concentration (5−100 μM; Figure 5B), and the data were fit to a straight line. The observed slope of −0.96 (R^2 = 0.986) indicates a nucleus size of 2, suggesting that bimolecular initiation in the presence of **1**(**2**) occurs at the same rate as subsequent monomer addition. This observation suggests that the first stage of Aβ 1−40 aggregation induced by **1**(**2**) is a downhill polymerization (i.e., a polymerization without a barrier due to nucleation) instead of a nucleated polymerization.

The behavior of the second stage of aggregation is more difficult to interpret. This process did not occur on short time scales when samples were agitated as described above; therefore, samples were prepared and the TfT fluorescence measured as described above, but they were agitated more frequently (5 s of shaking every 10 min). The first stage of aggregation still appeared to be a downhill polymerization under these conditions (slope −0.98 for log t_{50} vs log Aβ 1−40 concentration plot, R^2 = 0.99, data not shown). However, the second stage of aggregation was independent of Aβ 1−40 concentration (slope = −0.07 for log t_{50} vs log [Aβ] plot, R^2 = 0.27, data not shown). This is not consistent with either a nucleated or a downhill polymerization. The

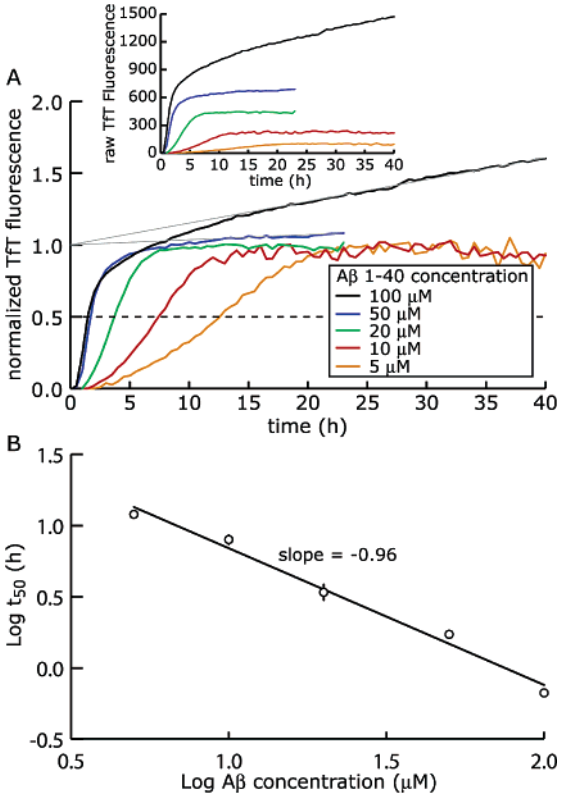

FIGURE 5: (A) The first stage of Aβ 1−40 (5 to 100 μM) aggregation (pH 7.4, 37 °C) with agitation (5 s of shaking every 30 min) in the presence of **1**(**2**) (50 μM) as detected by TfT fluorescence. Fluorescence is normalized to the value of the plateau phase for concentrations of **1**(**2**) from 5 to 20 μM. For higher concentrations, the linear portion of the plot between the first and second stages was extrapolated back to the ordinate and the intercept was set equal to 1. (B) Plot of the logarithm of t_{50} (time to 50% completion) vs the logarithm of the Aβ concentration. The slope of the line of best fit is −0.96 (R^2 = 0.99). Error bars represent one standard deviation above or below the mean.

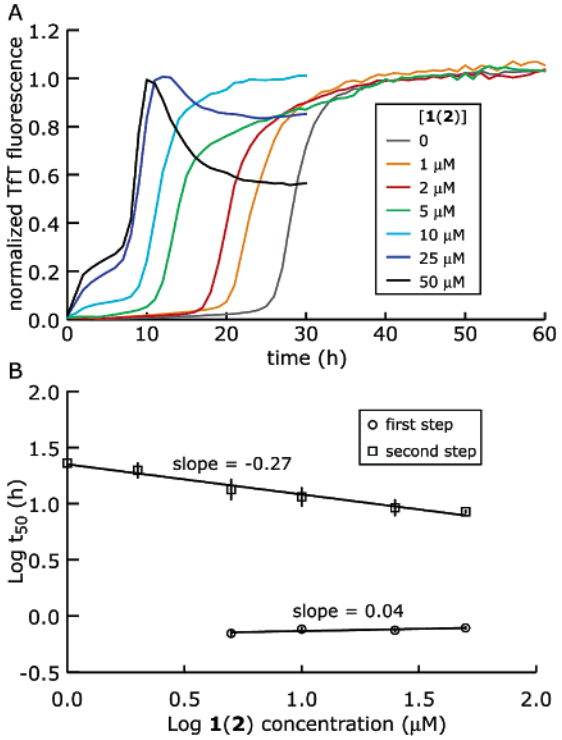

FIGURE 6: (A) Aβ 1−40 (50 μM) aggregation (pH 7.4, 37 °C) with agitation (5 s of shaking every 10 min) in the presence of **1**(**2**) (1 to 50 μM) as detected by TfT fluorescence. Fluorescence is normalized to the maximum fluorescence observed in a given reaction. (B) Plot of the logarithm of the t_{50} values for the first and second stages of the aggregation reactions in panel A vs the logarithm of the concentration of **1**(**2**). The slope of the line of best fit is 0.04 (R^2 = 0.67) for the first stage and −0.27 (R^2 = 0.97) for the second stage. Error bars represent one standard deviation above or below the mean.

sudden onset of the second stage of Aβ aggregation indicates that it could be an autocatalytic process, as suggested by Sabate and co-workers (*19*), and analogous to autocatalytic prion replication experimentally demonstrated by Bieschke (*20*), as proposed by Eigen (*21*) and modeled by Masel (*22*), in which breakage exposes new ends for fibril extension.

*Dependence of the Aβ 1−40 Aggregation Time Scale on **1(2)** Concentration Suggests that **1(2)** Forms Micelles.* The concentration of Aβ−**1**(**2**) adducts, and therefore the time scale of the Aβ 1−40 aggregation reaction, should depend on the concentration of **1**(**2**). Such a dependence, however, is not apparent either in previously published data (*7*) or in Figure 3A; the slope of a plot of log t_{50} for the first stage of aggregation vs log[**1**(**2**)] for these data is −0.17. Furthermore, in assays that were agitated more intensely (5 s of agitation every 10 min; Figure 6A), both the first and second stages of Aβ 1−40 (50 μM) aggregation exhibit weak dependencies of log t_{50} on log[**1**(**2**)] (Figure 6B).

The observations cited above suggest that the effective concentration of **1**(**2**) is independent of the total concentration of **1**(**2**). This can be rationalized by noting that **1**(**2**) forms micelles (see Figure 10, Supporting Information). Because **1**(**2**) forms micelles, the concentration of monomeric (nonmicellar) **1**(**2**) increases slowly as the total concentration of **1**(**2**) increases above the critical micelle concentration (CMC). The effect of **1**(**2**) therefore also increases slowly as the total concentration of **1**(**2**) increases. The CMC for **1**(**2**) is at most 100 nM and probably substantially lower (this is comparable to CMC values reported for cholesterol (*23*)).

*The Growth Rate of Aβ 1−40 Fibrils Is Unaffected by **1(2)**.* A second signature characteristic of nucleated polymerizations is that they can be accelerated by adding preformed fibrils (seeds) to the reaction, thereby obviating nucleation. This feature has been used to study the fibril growth process in the absence of confounding effects from nucleation (*24*). A seeded Aβ 1−40 aggregation assay was therefore used to assess the effect of **1**(**2**) on fibril growth. Seeds were obtained from an agitated (5 s of shaking every 10 min), unseeded Aβ 1−40 (50 μM) aggregation reaction carried out at 37 °C and pH 7.4 in the absence of **1**(**2**). The seeds were fragmented by 30 min of sonication. AFM images indicate that the seeds produced had a typical length of 50−100 nm (data not shown).

Solutions of Aβ 1−40 (50 μM), **1**(**2**) (0 to 50 μM), and TfT (20 μM) were prepared and allowed to preincubate (pH 7.4, 37 °C) for 2 min before fibrillar seeds (5, 10, or 20 wt %) were added, at which point sample agitation was initiated (5 s of shaking every 10 min). The TfT fluorescence was then measured at regular intervals (Figure 7A). Under these conditions, fibril elongation should dominate the formation of new fibrils (*24*). The early portions of the reaction profiles were fit to a line (Figure 7A). The slope of this line corresponded to the initial rate of the elongation reaction.

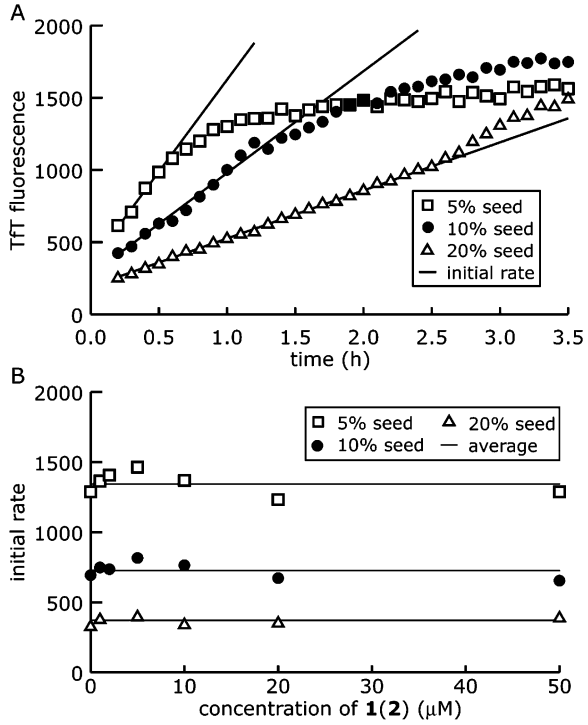

FIGURE 7: (A) Seeded (5, 10, or 20 wt %) Aβ 1−40 (50 μM) aggregation (pH 7.4, 37 °C) with agitation (5 s of shaking every 10 min) as detected by TfT fluorescence (arbitrary units). The slopes of the black lines are equal to the initial rates of the seeded aggregation reactions. (B) Dependence of the initial rates (arbitrary units/h) of seeded Aβ 1−40 aggregation reactions on the concentration of **1**(**2**). The gray lines represent the average values of the initial rates at a given seed concentration.

These initial rates were plotted against the concentration of **1**(**2**) for 5, 10, and 20 wt % seed concentration (Figure 7B). The initial rates increased with seed concentration but were independent of the concentration of **1**(**2**). This demonstrates that **1**(**2**) does not influence fibril growth; it must therefore exert its effect on Aβ aggregation through an initiation step.

Small Molecules that React with Aldehyde Functional Groups Abolish Acceleration of Aβ 1−40 Aggregation by 1(2). We have shown that **1**(**2**) forms a Schiff base with Aβ 1−40 (*7*). If Schiff base formation were mechanistically important, small molecule competitors that react with the aldehyde of **1**(**2**) and block Aβ−**1**(**2**) adduct formation should abolish its activity. Aminoguanidine, carnosine, pyridoxamine, hydralazine, and methoxyamine are aldehyde sequestering compounds that react with lipid peroxidation products such as 4-hydroxynonenal (*25*). These compounds (100 μM) were incubated with agitation (5 s of shaking every 10 min) with Aβ 1−40 (50 μM), **1**(**2**) (0, 10, or 50 μM) and TfT (20 μM) at 37 °C and pH 7.4. The t_{50} values for each of the reactions (based on the increase in TfT fluorescence) were determined (Figure 8; the plotted t_{50} values are for the second stage of the aggregation reaction because this is the only stage observed in the absence of **1**(**2**)). Four of the aldehyde sequestering drugs (aminoguanidine, carnosine, hydralazine, and methoxyamine) eliminated the aggregation-enhancing effect of **1**(**2**) at 10 μM. However, at a higher concentration of **1**(**2**) (50 μM) the aldehyde interceptors became less effective, as expected, supporting the hypothesis that the covalent attachment of **1**(**2**) to Aβ 1−40 is critical for the acceleration of Aβ fibrilization.

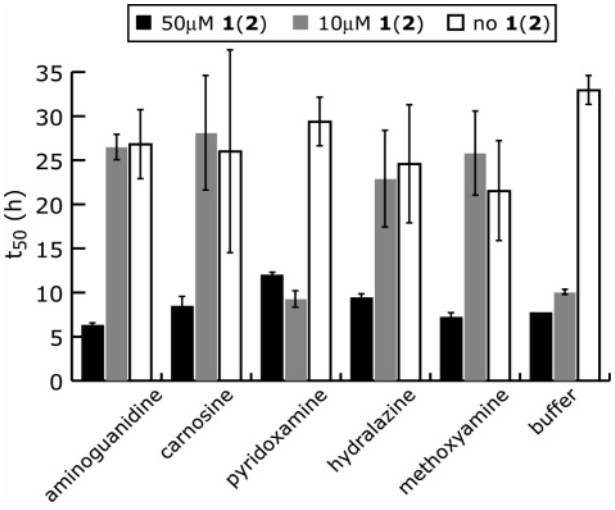

FIGURE 8: Bar graph of the t_{50} values of the second stage of Aβ 1−40 (50 μM) aggregation reactions (pH 7.4, 37 °C, 5 s of shaking every 10 min) at varying concentrations of **1**(**2**) (0, 10, or 50 μM) in the presence of an aldehyde sequestering drug (100 μM). Error bars represent standard deviations from triplicate experiments.

DISCUSSION

We have shown that Aβ aggregation is accelerated by **1**(**2**) (*7*). Covalent modification by these metabolites represents a possible chemical mechanism by which two known risk factors for AD, inflammation and hypercholesterolemia, can contribute to the pathogenesis of AD. The results in this work, taken together with our previous data (*7*), yield the following picture of metabolite-initiated Aβ 1−40 aggregation.

Incubating Aβ 1−40 with **1**(**2**) leads to the formation of Aβ−**1**(**2**) Schiff base adducts. This process occurs at low (<100 nM) concentrations of monomeric **1**(**2**), since the concentration of nonmicellar **1**(**2**) cannot be much larger than its CMC (which is at most 100 nM). The Aβ−**1**(**2**) adducts aggregate by a downhill polymerization to form small, spherical aggregates. Some unmodified Aβ is also recruited in this process, so that the aggregates consist of equal parts of modified and unmodified Aβ (*7*). The extent of aggregation, however, is proportional to the concentration of **1**(**2**). Under quiescent conditions, this is the only stage of metabolite-initiated Aβ amyloidogenesis observed on a convenient laboratory timescale. However, in agitated samples, **1**(**2**) accelerates a second stage of aggregation during which fibrils are formed. This stage continues until almost all of the Aβ (>90%), modified or unmodified, is consumed. Fibril formation occurs more rapidly in the presence of **1**(**2**) than in the absence, even at low concentrations of **1**(**2**). It is important to note that **1**(**2**) does not increase the fibril growth rate in the second stage of Aβ aggregation; rather, it is likely that the spherical aggregates are involved in the formation of new fibrils in a process that has some of the features of autocatalysis.

We have stated above that our results with **1**(**2**) and other metabolites provide a possible explanation for how hypercholesterolemia and inflammation can trigger sporadic AD. Beyond this, however, our results demonstrate that, in addition to primary sequence and environment, small molecules can determine whether a protein folds or misfolds. Specifically, we have shown that metabolite modification

of Aβ enables it to aggregate at nanomolar concentrations, providing an explanation for how Aβ could aggregate under physiological conditions, without invoking prior ideas that it needs to be concentrated 1000−10000-fold by some microenvironment in the brain to trigger a nucleated polymerization. Although we have focused on the effect of **1**(**2**) on Aβ misfolding, the phenomenon of metabolite-initiated protein misfolding is likely to occur with other proteins and other metabolites (for example, 4-hydroxynonenal also accelerates Aβ aggregation (*7*)), and it is likely that metabolite modification also plays a role in normal physiology and folding (for example, the N-terminal signaling moiety of Hedgehog must be covalently modified by cholesterol to function properly (*26*−*28*)). Metabolite modification and its influence on protein folding and misfolding could be an important determinant in many processes, both physiological and pathological.

ACKNOWLEDGMENT

We thank M. R. Ghadiri for use of his AFM.

SUPPORTING INFORMATION AVAILABLE

The disappearance of Aβ monomers and the formation of oligomers in early aggregation stages in the presence and absence of **1**, and micelle formation by **1** and by cholesterol were monitored by static and dynamic light scattering. This material is available free of charge via the Internet at http://pubs.acs.org.

REFERENCES

1. Mattson, M. P. (2004) Pathways towards and away from Alzheimer's disease, *Nature 430*, 631−639.
2. Kang, J., Lemaire, H. G., Unterbeck, A., Salbaum, J. M., Masters, C. L., Grzeschik, K. H., Multhaup, G., Beyreuther, K., and Muller-Hill, B. (1987) The precursor of Alzheimer's disease amyloid A4 protein resembles a cell-surface receptor, *Nature 325*, 733−736.
3. Haass, C., Koo, E. H., Mellon, A., Hung, A. Y., and Selkoe, D. J. (1992) Targeting of cell-surface beta-amyloid precursor protein to lysosomes: alternative processing into amyloid-bearing fragments, *Nature 357*, 500−503.
4. Sengupta, P., Garai, K., Sahoo, B., Shi, Y., Callaway, D. J., and Maiti, S. (2003) The amyloid beta peptide (Abeta(1−40)) is thermodynamically soluble at physiological concentrations, *Biochemistry 42*, 10506−10513.
5. Cannon, M. J., Williams, A. D., Wetzel, R., and Myszka, D. G. (2004) Kinetic analysis of beta-amyloid fibril elongation, *Anal. Biochem. 328*, 67−75.
6. Harper, J. D., and Lansbury, P. T., Jr. (1997) Models of amyloid seeding in Alzheimer's disease and scrapie: mechanistic truths and physiological consequences of the time-dependent solubility of amyloid proteins, *Annu. Rev. Biochem. 66*, 385−407.
7. Zhang, Q., Powers, E. T., Nieva, J., Huff, M. E., Dendle, M. A., Bieschke, J., Glabe, C. G., Eschenmoser, A., Wentworth, P., Jr., Lerner, R. A., and Kelly, J. W. (2004) Metabolite-initiated protein misfolding may trigger Alzheimer's disease, *Proc. Natl. Acad. Sci. U.S.A. 101*, 4752−4757.
8. Wentworth, P., Jr., Nieva, J., Takeuchi, C., Galve, R., Wentworth, A. D., Dilley, R. B., DeLaria, G. A., Saven, A., Babior, B. M., Janda, K. D., Eschenmoser, A., and Lerner, R. A. (2003) Evidence for ozone formation in human atherosclerotic arteries, *Science 302*, 1053−1056.
9. Hartley, D. M., Walsh, D. M., Ye, C. P., Diehl, T., Vasquez, S., Vassilev, P. M., Teplow, D. B., and Selkoe, D. J. (1999) Protofibrillar intermediates of amyloid beta-protein induce acute electrophysiological changes and progressive neurotoxicity in cortical neurons, *J. Neurosci. 19*, 8876−8884.
10. Walsh, D. M., Hartley, D. M., Kusumoto, Y., Fezoui, Y., Condron, M. M., Lomakin, A., Benedek, G. B., Selkoe, D. J., and Teplow, D. B. (1999) Amyloid beta-protein fibrillogenesis. Structure and biological activity of protofibrillar intermediates, *J. Biol. Chem. 274*, 25945−25952.
11. Walsh, D. M., Klyubin, I., Fadeeva, J. V., Cullen, W. K., Anwyl, R., Wolfe, M. S., Rowan, M. J., and Selkoe, D. J. (2002) Naturally secreted oligomers of amyloid b protein potently inhibit hippocampal long-term potentiation in vivo, *Nature 416*, 535−539.
12. Kirkitadze, M. D., Bitan, G., and Teplow, D. B. (2002) Paradigm shifts in Alzheimer's disease and other neurodegenerative disorders: the emerging role of oligomeric assemblies, *J. Neurosci. Res. 69*, 567−577.
13. Lambert, M. P., Barlow, A. K., Chromy, B. A., Edwards, C., Freed, R., Liosatos, M., Morgan, T. E., Rozovsky, I., Trommer, B., Viola, K. L., Wals, P., Zhang, C., Finch, C. E., Krafft, G. A., and Klein, W. L. (1998) Diffusible, nonfibrillar ligands derived from Ab1−42 are potent central nervous system neurotoxins, *Proc. Natl. Acad. Sci. U.S.A. 95*, 6448−6453.
14. Gong, Y., Chang, L., Viola, K. L., Lacor, P. N., Lambert, M. P., Finch, C. E., Krafft, G. A., and Klein, W. L. (2003) Alzheimer's disease-affected brain: presence of oligomeric A beta ligands (ADDLs) suggests a molecular basis for reversible memory loss, *Proc. Natl. Acad. Sci. U.S.A. 100*, 10417−10422.
15. Kayed, R., Head, E., Thompson, J. L., McIntire, T. M., Milton, S. C., Cotman, C. W., and Glabe, C. G. (2003) Common Structure of Soluble Amyloid Oligomers Implies Common Mechanism of Pathogenesis, *Science 300*, 486−489.
16. Caughey, B., and Lansbury, P. T., Jr. (2003) Protofibrils, pores, fibrils, and neurodegeneration: Separating the responsible protein aggregates from the innocent bystanders, *Annu. Rev. Neurosci. 26*, 267−298.
17. LeVine, H., 3rd. (1999) Quantification of beta-sheet amyloid fibril structures with thioflavin T, *Methods Enzymol. 309*, 274−284.
18. Jarrett, J. T., and Lansbury, P. T., Jr. (1993) Seeding "one-dimensional crystallization" of amyloid: A pathogenic mechanism in Alzheimer's disease and scrapie? *Cell 73*, 1055−1058.
19. Sabate, R., Gallardo, M., and Estelrich, J. (2003) An autocatalytic reaction as a model for the kinetics of the aggregation of beta-amyloid, *Biopolymers 71*, 190−195.
20. Bieschke, J., Weber, P., Sarafoff, N., Beekes, M., Giese, A., and Kretzschmar, H. (2004) Autocatalytic self-propagation of misfolded prion protein, *Proc. Natl. Acad. Sci. U.S.A. 101*, 12207−12211.
21. Eigen, M. (1996) Prionics or the kinetic basis of prion diseases, *Biophys. Chem. 63*, A1−18.
22. Masel, J., Jansen, V. A., and Nowak, M. A. (1999) Quantifying the kinetic parameters of prion replication, *Biophys. Chem. 77*, 139−152.
23. Haberland, M. E., and Reynolds, J. A. (1973) Self-association of cholesterol in aqueous solution, *Proc. Natl. Acad. Sci. U.S.A. 70*, 2313−2316.
24. Collins, S. R., Douglass, A., Vale, R. D., and Weissman, J. S. (2004) Mechanism of prion propagation: amyloid growth occurs by monomer addition, *PLoS Biol. 2*, 1582−1590.
25. Burcham, P. C., Kaminskas, L. M., Fontaine, F. R., Petersen, D. R., and Pyke, S. M. (2002) Aldehyde-sequestering drugs: tools for studying protein damage by lipid peroxidation products, *Toxicology 181*−*182*, 229−236.
26. Porter, J. A., Young, K. E., and Beachy, P. A. (1996) Cholesterol modification of hedgehog signaling proteins in animal development, *Science 274*, 255−259.
27. Mann, R. K., and Beachy, P. A. (2000) Cholesterol modification of proteins, *Biochim. Biophys. Acta 1529*, 188−202.
28. Lewis, P. M., Dunn, M. P., McMahon, J. A., Logan, M., Martin, J. F., St-Jacques, B., and McMahon, A. P. (2001) Cholesterol modification of sonic hedgehog is required for long-range signaling activity and effective modulation of signaling by Ptc1, *Cell 105*, 599−612.

BI0501030